Memoirs the Faculty of Engineering, Nagoya University
Vol. 32, No. 2 (1980) — Research Report —

ON THE TURBULENT BOUNDARY LAYER ON A SPINNING TAIL BODY IN AN AXIAL FLOW

——A Simple Calculation and Experiments in the Case of High Speed Ratio——

IKUO NAKAMURA, SHINTARO YAMASHITA, and KUMIO YAMAMOTO*

Department of Mechanical Engineering

(Received October 31, 1980)

Abstract

A simple and practical method is presented to calculate the turbulent boundary layer on a rotating cone with the radius decreasing toward downstream. Fundamental assumptions are the generalized quasi-collaterality and a skin friction law of power law type. Predicted results of the method agree excellently with the experimental value of momentum thicknesses. Measurements of Reynolds stress have been performed by use of two types of rotated hot wires. The three components of turbulent intensities show very large growth with the rotating speed of the cone. Also the Reynolds shear stress components exhibit big effect of the speed ratio. Turbulent energy production and transport terms computed from measured quantities show the importance of the novel terms.

1. Introduction

When the boundary layer theory is applied to practical problems, in many cases, only values of skin friction and various integrated thicknesses are required. From this point of view many sophisticated prediction methods[1] recently developed for the boundary layer equation give too much results needed for the problems to be

* Present Adress: Toyota Central Research & Development Laboratories, Inc.

solved. And these new methods are too complicated for usual designers of machinery to master them and to apply them to their daily problems.

The boundary layers on various axisymmetric bodies spinning in axial flows are the typical real problems in the fluids engineering and have been studied by many authors so far.[2~6] New methods of the boundary layer theory above mentioned also have been applied to these problems actively but they are complicated and the calculated results do not completely well agree with the experimental results.[7~10]

This report concerns mainly with the simplified treatment on the momentum integral equations of the boundary layer developing on a conical body with the radius decreasing toward downstream which is spinning in an axial stream with constant pressure. Basic assumptions are generalized quasi-collaterality of the velocity distribution in the boundary layer and a power law of the skin friction. The construction of the method is an extension of Parr's method[3] for solving the momentum integral equation to the thick boundary layer on which the effect of curvature is important. The final form of the present method is rather simple and easy to apply but the calculated results agree well with the experiments.

Experiments also have been performed and especially the attention has been focused on the effect of the speed ratio on the turbulence structure. Reynolds stress components were measured by use of two rotated hot wire probes. The results show strong effect of the speed ratio which seems to be difficult to explain on the basis of an eddy viscosity. In what follows experimental results mainly at the high speed ratio will be presentd. Contents of this paper relate intimately with the previous paper.[5]

2. The Momentum Integral Equations and Their Solution

2. 1. Fundamental equations

Consider a turbulent boundary layer developing on a conical surface with decreasing radius toward downstream and the cone rotates in a flow parallel to generators of the cone as shown in Fig. 1. The boundary layer on this part of the body is subjected by the centrifugal force which influences the boundary layer as an adverse pressure gradient and the boundary layer becomes thick at the rear part of the body comparing to the cone radius. These factors complicate the character of the boundary layer. On the nose part of the body the boundary layer is thin and laminar, and a series solution for the layer is given by the authors.[4] Thin turbulent boundary layer on a spinning body of revolution in an axial flow is treated by a momentum integral method by Parr and it gives useful results.[3]

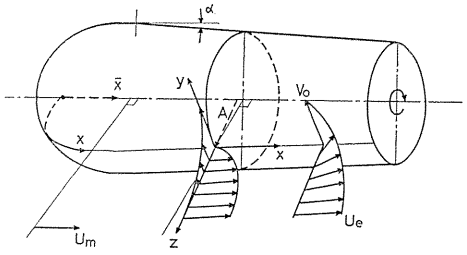

Fig. 1. Flow configuration and the coordinate system.

We take x as the distance along the meridian of the body, y the azimuthal angle, z the distance from the body surface. Let U, V and W indicate average velocity components, and u, v and w indicate fluctuating velocity components in the

x, y and z directions respectively. The Reynolds equations and the continuity equation expressed in this coordinate are

$$DU+\frac{\lambda}{R}V^2=-\frac{1}{\rho}\frac{\partial P}{\partial x}+\nu\left(\nabla^2 U-\frac{\lambda^2}{R^2}U+\frac{\lambda}{R^2}W\right)-$$
$$-\left\{\frac{1}{R}\frac{\partial(R\overline{u^2})}{\partial x}+\frac{\lambda}{R}\overline{v^2}+\frac{1}{R}\frac{\partial(R\overline{uw})}{\partial z}\right\}, \tag{1}$$

$$DV-\lambda\frac{UV}{R}+\frac{VW}{R}=\nu\left(\nabla^2 V-\frac{\lambda^2}{R^2}V-\frac{V}{R^2}\right)-\left\{\frac{1}{R^2}\frac{\partial(R^2\overline{uv})}{\partial x}+\frac{1}{R^2}\frac{\partial(R^2\overline{vw})}{\partial z}\right\}, \tag{2}$$

$$DW-\frac{V^2}{R}=-\frac{1}{\rho}\frac{\partial P}{\partial z}+\nu\left(\nabla^2 W-\frac{W}{R^2}+\frac{\lambda}{R^2}U\right)-$$
$$-\left\{\frac{\partial(\overline{uw})}{\partial x}-\frac{\lambda}{R}\overline{uw}+\frac{\partial\overline{w}^2}{\partial z}+\frac{1}{R}(\overline{w}^2-\overline{v}^2)\right\}, \tag{3}$$

$$\frac{\partial}{\partial x}(RU)+\frac{\partial}{\partial z}(RW)=0, \tag{4}$$

where $D=U\cdot\partial/\partial x+W\cdot\partial/\partial z$, and $\nabla^2=\partial^2/\partial x^2+\partial^2/\partial z^2-\lambda/R\cdot\partial/\partial x+1/R\cdot\partial/\partial z$.
R represents the distance from an any point considered to the rotating axis along the z coordinate axis. λ is inclination of the conical surface, $\lambda=-\partial R/\partial x=\tan\alpha$ and other nomenclature is conventional one.

From these equations, we will derive the boundary layer equations applicable to the thick boundary layer comparing to the body radius. Here we will use the order estimation method after Hinze.[11] Let L_1 and L_3 be the representative lengths in the x and z directions respectively and let $\overline{U}_1$, $\overline{U}_2$ and $\overline{U}_3$ be the velocity scales in the x, y and z directions respectively. In the present problem we consider the case where the boundary layer thickness δ is the same order of magnitude to the body radius, then we have following relationship,

$$\delta\sim A\sim L_3, \tag{5}$$

where A stands for the radius of main curvature of the conical surface as shown in Fig. 1. Using A, R is represented as $R=A+z$. Although δ is assumed to be the same order as A, let the range of x expand much larger than δ, that is,

$$L_3/L_1\ll 1. \tag{6}$$

Then from the continuity equation we have $\overline{U}_3/\overline{U}_1\ll 1$. Furthermore we assume that every fluctuating velocity components have the same order of magnitude v^2 and components of Reynolds stress are represented as $\overline{u_iu_j}\sim R_{ij}v^2$, R_{ij} is the correlation tensor, then the following order estimation can be done,

$$\left.\begin{aligned} &\overline{u}^2\sim\overline{v}^2\sim\overline{w}^2\sim\boldsymbol{v}^2,\\ &\overline{uv}\sim\boldsymbol{R}_{12}\boldsymbol{v}^2,\quad \overline{uw}\sim\boldsymbol{R}_{13}\boldsymbol{v}^2,\quad \overline{vw}\sim\boldsymbol{R}_{23}\boldsymbol{v}^2,\quad \boldsymbol{R}_{ij}\sim 1. \end{aligned}\right\} \tag{7}$$

The ratio of the inclination of cone surface λ to R is at most order of $1/L_1$.

Using the relationships obtained above, we estimate the orders of magnitude of the terms of Eqs. (1) to (3). We take $\overline{U}_1^2/L_1\sim\overline{U}_2^2/L_1\sim 1$ for convenience. If we assume that the terms of the fluctuating velocity components are not so great that the equations are balanced only by these terms and the terms of the pressure gradients, then we must require that $\boldsymbol{v}^2/L_3\sim 1$. Retaining the terms of order 1, we have following turbulent boundary layer equations.

$$\left.\begin{aligned} &\rho DU=-\frac{\partial P}{\partial x}-\rho\lambda\frac{V^2}{R}+\frac{1}{R}\frac{\partial(R\tau_x)}{\partial z},\\ &\rho\left(DV+\frac{VW}{R}\right)=\rho\lambda\frac{UV}{R}+\frac{1}{R^2}\frac{\partial(R^2\tau_y)}{\partial z},\\ &\rho\frac{V^2}{R}=\frac{\partial P}{\partial z}+\rho\left\{\frac{\partial\overline{w}^2}{\partial z}+\frac{1}{R}(\overline{w}^2-\overline{v}^2)\right\}, \end{aligned}\right\} \tag{8a, b, c}$$

$$\frac{\partial(RU)}{\partial x}+\frac{\partial(RW)}{\partial z}=0, \tag{9}$$

where τ_x and τ_y are components of the shear stress in the x and y directions respectively expressed as,

$$\tau_x=\mu\frac{\partial U}{\partial z}-\rho\overline{uw},\quad \tau_y=\mu\left(\frac{\partial V}{\partial z}-\frac{V}{R}\right)-\rho\overline{vw}. \tag{10a, b}$$

Boundary conditions to be satisfied are

$$\left.\begin{aligned} &z=0;\quad U=W=u=v=w=0,\quad V=V_0=a\omega,\\ &z\to\infty;\quad U\to U_e,\quad V,\ u,\ v,\ w\to 0, \end{aligned}\right\} \tag{11a, b}$$

where U_e is main flow velocity outside of the boundary layer and a is the local radius of the cone.

Now we will derive the momentum integral equations. Integration of Eq. (8c) yields

$$\frac{P-P_e}{\rho}=\int_\delta^z\left[\frac{V^2}{R}-\left\{\frac{\partial\overline{w}^2}{\partial z}+\frac{1}{R}(\overline{w}^2-\overline{v}^2)\right\}\right]dz. \tag{12}$$

Then the pressure gradient in the streamwise direction is

$$-\frac{1}{\rho}\frac{\partial P}{\partial x}=-\frac{1}{\rho}\frac{dP_e}{dx}+\frac{\partial}{\partial x}\int_z^\delta\left[\frac{V^2}{R}-\left\{\frac{\partial\overline{w}^2}{\partial z}+\frac{1}{R}(\overline{w}^2-\overline{v}^2)\right\}\right]dz. \tag{13}$$

Introducing Eq. (13) into Eq. (8a) and it times R and Eq. (8b) times R^2 and integrating these equations by z from zero to δ considering the continuity equation, we obtain following two momentum integral equations,

$$\frac{d}{dx}\{AU_e^2(\Theta_x+\theta_r'-\theta_{rr}')\}+A\Delta_x U_e\frac{dU_e}{dx}+\frac{d}{dx}\{AV_0^2(\Theta_{yy}+\theta_{yy}')\}-$$

$$-\lambda\{V_0^2(\Theta_y-\Theta_{yy}'-\theta_{yy}'')-U_e^2(\theta_r''-\theta_{rr}'')\}=A\frac{\tau_{ox}}{\rho}, \tag{14}$$

$$\frac{d}{dx}(A^2U_eV_0\Theta_{xy})=-A^2\frac{\tau_{oy}}{\rho}, \tag{15}$$

where τ_{ox} and τ_{oy} are components of wall shear stress in the x and y directions respectively. The various integrated thicknesses appeared in the above equations are defined by following equations,

$$\left.\begin{aligned}&\Theta_x=\int_0^\delta\frac{U}{U_e}\left(1-\frac{U}{U_e}\right)\frac{R}{A}dz,\quad \Theta_y=\int_0^\delta\left(\frac{V}{V_0}\right)^2dz,\\&\Theta_{xy}=\int_0^\delta\frac{U}{U_e}\frac{V}{V_0}\left(\frac{R}{A}\right)^2dz,\quad \Delta_x=\int_0^\delta\left(1-\frac{U}{U_e}\right)\frac{R}{A}dz,\end{aligned}\right\} \tag{16}$$

$$\Theta_{yy}=\int_0^\delta\frac{R}{A}\int_z^\delta\frac{1}{R'}\left(\frac{V}{V_0}\right)^2dz'dz,\quad \Theta_{yy}'=\int_0^\delta\int_z^\delta\frac{1}{R'}\left(\frac{V}{V_0}\right)^2dz'dz, \tag{17}$$

$$\left.\begin{aligned}&\theta_r'=\int_0^\delta\frac{\overline{w}^2}{U_e^2}\frac{R}{A}dz,\quad \theta_{rr}'=\int_0^\delta\frac{R}{A}\int_z^\delta\frac{1}{R'}\frac{\overline{w}^2}{U_e^2}dz'dz,\\&\theta_{yy}'=\int_0^\delta\frac{R}{A}\int_z^\delta\frac{1}{R'}\frac{\overline{v}^2}{V_0^2}dz'dz,\quad \theta_r''=\int_0^\delta\frac{\overline{w}^2}{U_e^2}dz,\\&\theta_{rr}''=\int_0^\delta\int_z^\delta\frac{1}{R'}\frac{\overline{w}^2}{U_e^2}dz'dz,\quad \theta_{yy}''=\int_0^\delta\int_z^\delta\frac{1}{R'}\frac{\overline{v}^2}{V_0^2}dz'dz,\end{aligned}\right\} \tag{18}$$

where $R'=A+z'$. These definitions contain the effect of curvature.

Θ_x and Θ_y represent the momentum thicknesses in the x and y directions respectively. Θ_{xy} is the angular momentum thickness and Δ_x is the displacement thickness in the x direction. The effect of centrifugal force produced by the rotation of the cone is expressed by Θ_{yy} and Θ_{yy}'. Various thicknesses like θ_r', θ_{rr}', θ_{yy}', θ_r'', θ_{rr}'', θ_{yy}'' represent the effect of Reynolds normal stresses. Hinze's order estimation method used here eliminates the terms related to $\overline{u^2}$ and then we have no thicknesses corresponding to it.

2. 2. Fundamental assumptions

To solve the momentum integral equation for the two-dimensional turbulent boundary layer it is required to make two assumptions, one of which is a some law of the skin friction and the other shows a relationship of the ratio of integrated thicknesses, the shape factor, to the other parameters. The differences between various methods of solution occur mainly from the variance of the equations for the shape factor.[12] The similar assumptions are also needed in the present problem.

Unlike two-dimensional problem two momentum integral equations should be solved, then at first we will consider the relationship between the velocity profiles in the x and y directions. Frequently Mager's relationship[13] is used for the usual

three-dimensional turbulent boundary layer but it is not appropriate for the present problem. In the laminar boundary layer on a rotating cylinder in an axial constant-pressure flow the velocity profiles in the x and y directions have exactly the following relationship, so called quasi-collaterality,[4]

$$\frac{V}{V_0}=1-\frac{U}{U_e}. \tag{19}$$

In this case streamwise velocity distribution is Blasius profile. Parr[3] assumes that Eq. (19) holds in any boundary layer, laminar or turbulent, on the spinning body of arbitrary shape. Indeed Eq. (19) has been proved approximately in many cases.[14] We will generalize the concept of the quasi-collaterality.

In the previous paper[4] we have treated this problem from the geometrical point of view, here we will use the vector algebra. Since Eq. (19) means the velocity vector in the boundary layer is coplanar with the relative main flow direction, it may be expected that the analysis will be simplified by use of the coordinate system fixed to the rotating body. The position vector of the point considered is $\boldsymbol{r}$ which spans from the axis of rotation. The inviscid relative velocity vector $\boldsymbol{U}_R$ at that point to the coordinate system rotating with the body is

$$\boldsymbol{U}_R=\boldsymbol{U}_e-\boldsymbol{\omega}\times\boldsymbol{r}, \tag{20}$$

where $\boldsymbol{U}_e$ represents the velocity vector of the inviscid flow viewed from the stationary coordinate and $\boldsymbol{\omega}$ is the angular velocity of the spinning body.

Let $\boldsymbol{U}$ be the velocity in the boundary layer in the stationary frame and $\boldsymbol{U}_{rel}$ be the one relative to the rotating coordinate then the following equation exists,

$$\boldsymbol{U}_{rel}=\boldsymbol{U}-\boldsymbol{\omega}\times\boldsymbol{r}. \tag{21}$$

The generalized quasi-collaterality holds true if the plane made of $\boldsymbol{U}_R$ and $\boldsymbol{r}$ contains $\boldsymbol{U}_{rel}$. The condition for the property is

$$\boldsymbol{U}_{rel}\cdot(\boldsymbol{r}\times\boldsymbol{U}_R)=0. \tag{22}$$

If this equation is expressed by the components in the present coodinate system, we obtain

$$\frac{A}{R}\frac{V}{V_0}=1-\frac{U}{U_e}. \tag{23}$$

If $\delta\ll A$ Eq. (23) reduces to Eq. (19), since $R=A+z$.

As mentioned in the following section Eq. (23) depicts the experimental results, then it will be taken as a fundamental assumption to obtain the solution of momentum integral equations.

Now we will consider a skin friction law. For the two-dimensional boundary layer a power law is frequently adopted,[15] that is,

$$\frac{\tau_0}{\rho U_e^2}=\frac{m}{(U_e\theta_x/\nu)^n} \tag{24}$$

where m and n are empirical constants. Parr[3] assumes Eq. (24) for the thin boundary layer on a rotating body in axial flow, but there means τ_0 a resultant wall

shear stress and $U_e/\cos\varphi$ is used instead of U_e where φ is the angle between τ_0 and x-axis. Furthermore he assumes Eq. (19) is valid in the whole boundary layer and obtains

$$\frac{\tau_{ox}}{\rho U_e^2}=\frac{m(1+\Omega^2)^{(1-n)/2}}{(U_e\theta_x/\nu)^n},\quad \frac{\tau_{oy}}{\rho V_0^2}=\frac{-m\Omega^{n-1}(1+\Omega^2)^{(1-n)/2}}{(V_0\theta_{xy}/\nu)^n}, \tag{25a, b}$$

where m and n are the same as those of the flat-plate boundary layer. In the case of thick boundary layer Eqs. (25 a, b) can not be used. Considering the form of Eq. (25 b) we assume for τ_{0y} using Θ_{xy} the following expression,

$$\frac{\tau_{oy}}{\rho V_0^2}=\frac{-m\Omega^{n-1}(1+\Omega^2)^{(1-n)/2}}{(V_0\theta_{xy}/\nu)^n}, \tag{26}$$

where m and n are, however, different values corresponding to the flat plate. This is evident from the fact that the log-law of the two-dimensional flow is not valid for the present flow.[4] It seems that τ_{0y} is easier to determine by use of Eq. (15) with measured values of Θ_{xy} and then m and n were evaluated. The assumption of generalized quasi-collaterality gives following equations,

$$\frac{\tau_{ox}}{\tau_{oy}}=\frac{\mu(\partial U/\partial z)_{z=0}}{\mu(\partial V/\partial z-V/R)_{z=0}}=-\frac{U_e}{V_0}=-\frac{1}{\Omega}, \tag{27}$$

$$\therefore\quad \frac{\tau_{ox}}{\rho U_e^2}=\frac{m\Omega^n(1+\Omega^2)^{(1-n)/2}}{(V_0\theta_{xy}/\nu)^n}. \tag{28}$$

The most important terms in the momentum integral equations are Θ_x and Θ_{xy} but there remain rather many thicknesses to be determined. At first we accept the experimental results that Θ_{yy} is very small and can be neglected. Although among the terms having λ in Eq. (14) Θ_y is not negligible whereas the other terms are small, the value of λ of this cone is so small that we eliminate these terms. Fortunately in the present we will compare the calculation with the constant pressure case and so Δ_x is immaterial. Of course inclusion of the term $A\Delta_x U_e dU_e/dx$ introduces very difficult problem about the shape factor. Since, in the boundary layer not very near the separation point, Reynolds normal stresses can usually be neglected, we also do not consider them.

From the above consideration we obtain final equations to be solved as follows,

$$\frac{d\bar{\theta}_x}{d\bar{x}}=\frac{m\Omega^{1+n}(1+\Omega^2)^{(1-n)/2}}{\bar{\theta}_{xy}{}^n}, \tag{29a}$$

$$\frac{d\bar{\theta}_{xy}}{d\bar{x}}=\frac{m\Omega^{1+n}(1+\Omega^2)^{(1-n)/2}}{\bar{\theta}_{xy}{}^n}+\frac{2\lambda\bar{\theta}_{xy}}{R_A}, \tag{29b}$$

where $\bar{x}=U_e x/\nu$, $\bar{\theta}_x=V_0\Theta_x/\nu$, $\bar{\theta}_{xy}=V_0\Theta_{xy}/\nu$, and $R_A=AU_e/\nu$.

The values of m and n are determined from the experimental results in the case of $Re=8\times10^4$ where the values of τ_{oy} have been estimated. We obtain

$$m=0.00282,\quad n=0.0352. \tag{30a, b}$$

Equations (29a, b) are solved numerically.

3. Experimental Results and Discussion

3. 1. Experimental apparatus and procedures

A wind tunnel used is a suction type with inner diameter 350 mm. A rotating body is set in the wind tunnel in order to assure the zero pressure gradient in the measuring stations and then only the effect of inclined cone surface will appear in the boundary layer. Geometry of the conical part and measuring stations are shown in Fig. 2. U_m and P_m are reference main flow velocity and pressure respectively. They have been measured by a total and a static pressure tubes.

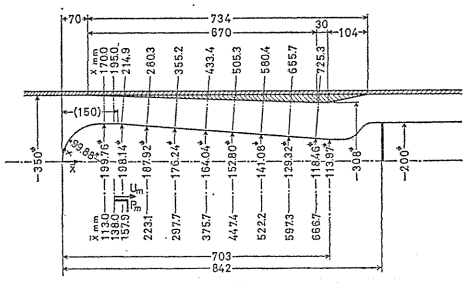

Fig. 2. The rotating body and measuring stations.

Mean flow velocity has been determined by a conventional I-type hot wire probe. The probe has been rotated around the inferred mean flow direction and the readings have been treated by use of the least square method. Reynolds stress components have been obtained by use of both a rotated I-probe and a rotated slanted-wire probe which is specially designed[5]. In principle Reynolds stress components can be measured by rotation of only one slanted-wire probe but this method has rather large error coming from the probe shape. Considering this error we have calculated the Reynolds stresses by means of the least square using the data obtained by two rotated probes. The inclination angle of the slant wire has been determined by the variation of the output obtained by the probe rotating in a uniform flow. In what follows the results mainly in the case of high speed ratio will be shown. Various profiles in the case of smaller speed ratio are presented in the previous paper[5].

3. 2. Comparison of the theory and the experimental results

In order to calculate Eqs. (29 a, b) we need the initial values of Θ_x and Θ_{xy}. Although it is desirable to calculate the laminar boundary layer from the stagnation point and to predict the transition point and then to determine the initial values of

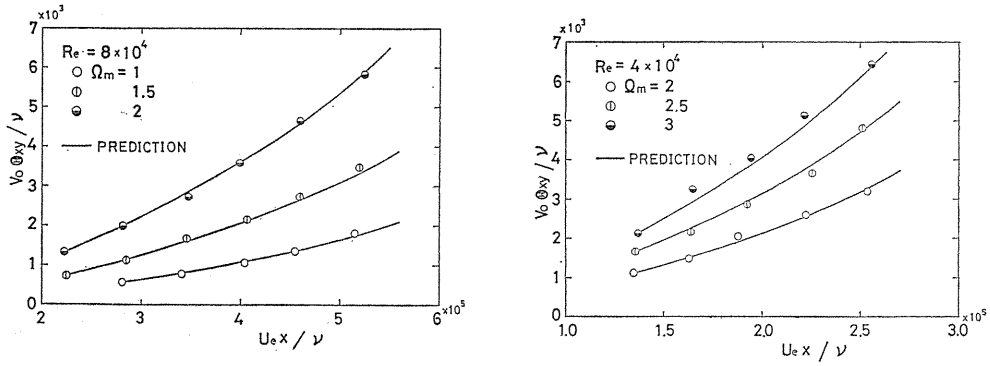

Fig. 3. (a), (b) Comparison of the theory with the experimental values of θ_{xy}.

Eqs. (29 a, b), such a calculation is impossible for the present state of art. So we have used the experimental values of Θ_x and Θ_{xy} for the initial values of the computation.

Figures 3 (a) and (b) show the calculated results of Θ_{xy} at $R_e=8\times10^4$ and 4×10^4 together with the experimental results respectively. Figure 3 (a) exhibits excellent agreement between the theory and the experiment. This is plausible because of the process to determine the values of m and n. The data in the case of $R_e=4\times10^4$ at the high speed ratio is independent of the determination of m and n. Figure 3 (b) shows, therefore, that the theory can predict the variation of Θ_{xy} at the high speed ratio.

Comparisons of Θ_x are shown in Figs. 4 (a) and (b) for $R_e=8\times10^4$ and 4×10^4 respectively. The theory predicts very well the development of Θ_x in the cases of $\Omega_m=1.0$ and 1.5. When the speed ratio reaches up to two, there appears slight discrepancy between the theoretical value and the experimental one. At the highest value of the speed ratio the discrepancy is appreciable as seen in Fig. 4 (b).

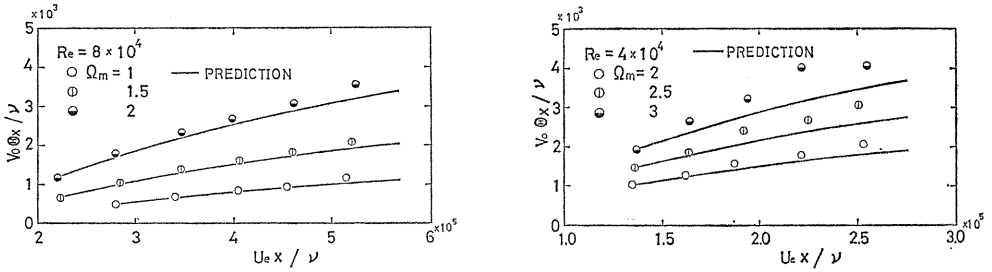

Fig. 4. (a), (b) Comparison of the theory with the experimental values of θ_x.

Above figures indicate that the present method can predict very well the two important momentum thicknesses of the complex rotating boundary layer in spite of its simplicity. A possible improvement of this method is to take the effects of the high speed ratio and the pressure gradient into account. When the body rotates at high speed, the terms including λ which are neglected in this calculation will become important.

3. 3. Mean velocity profiles

Development of the mean velocity profile in the boundary layer gives one of the most important aspects of the boundary layer. Figure 5 shows velocity profiles in the case of the highest speed ratio. The main flow velocity outside of the layer, the peripheral velocity of the cone surface, and Θ_x are used for the non-dimensional presentations of the velocity components in the x direction, y direction and the distance from the wall respectively. In this expression, velocity profiles are nearly similar as a whole but

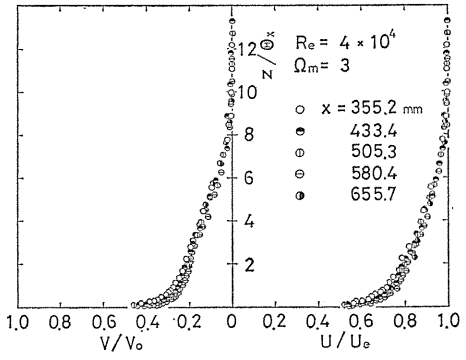

Fig. 5. Mean velocity profiles.

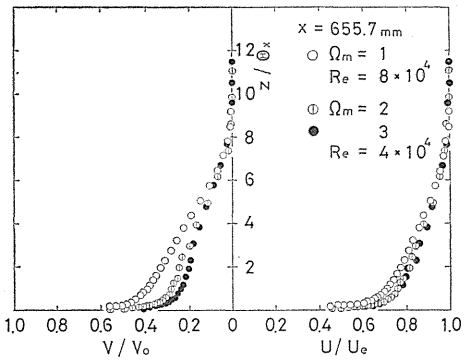

Fig. 6. Variation of the mean velocity profiles with the speed ratio.

some variations of the profiles are appreciable in the near-wall region. In the case of $\Omega_m=2$ at $R_e=8\times10^4$ of the previous paper[5], it was shown that the profiles expressed by the same coordinate were well similar in the azimuthal direction, but the velocity profiles in the x direction varied relatively large.

In the previous paper[5] a comparison is made between the mean velocity profiles on a rotating cylinder with a constant radius and ones on the same rotating cone as the present experiment. Here we will investigate the effect of the speed ratio on the velocity profiles on the rotating cone. Figure 6 shows this effect in the section of $x=655.7$ mm. In the figure velocity profiles in the cases of two Reynolds numbers are shown but the effect of the difference in the Reynolds number is immaterial. The velocity profiles in the x direction shown in the righthand side of the figure exhibits relatively accelerated shape with increasing the speed ratio. But save for the near-wall region the absolute value of the U-velocity component in the boundary layer decreases with increasing the speed ratio. This is due to both the rapid development of the boundary layer at the high speed ratio and the decelerating effect of the centrifugal force term, $-\rho\lambda V^2/R$, appeared in the righthand side of Eq. (8a).

Large influence of the speed ratio on the velocity profiles in the azimuthal direction is clearly shown in the lefthand side of Fig. 6. The change in the absolute value of the velocity component with the speed ratio is obscured in this figure because of the non-dimensional representation. One of the effects of the rotation on this boundary layer is produced by Coriolis-like force noted in the previous paper[5]. This is represented by the term $\rho\lambda UV/R$ appeared in Eq. (8b) and it accelerates the fluid in the boundary layer in the azimuthal direction. However the net dynamical effect of this force is similar to the effect exerted by the adverse pressure gradient on the U-velocity component. It can be recognized from the variation of the gradient of the azimuthal velocity profile with the speed ratio around $z/\Theta_x=2$. The absolute value of this gradient at that place decreases with increasing the speed ratio and this change is similar to the one appearing in the $\partial U/\partial y$ (y: normal to the wall) of the two-dimensional boundary layer affected by the adverse pressure gradient.

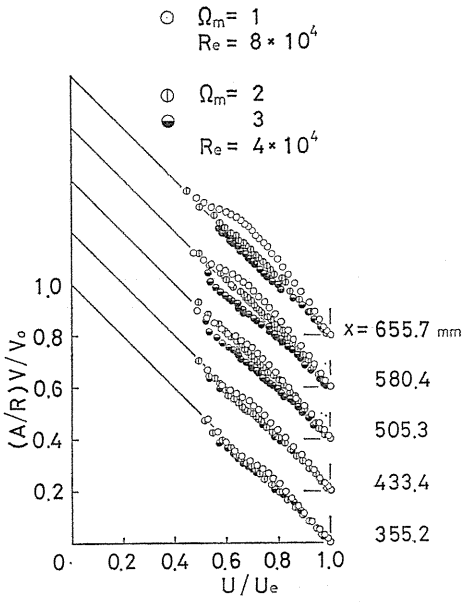

Fig. 7. Polar plots of velocity profiles.

Generalized quasi-collaterality assum-

ed as one of the fundamental assumptions for the calculation in Chap. 2 is checked in Fig. 7. For the sake of convenience the profiles in the case of the lower speed ratio is shown in the same figure again. An inference was made in the previous paper[5] that the polar plot of the velocity distribution will bend downward when the speed ratio is increased. The plot at the sections $x=505.3\sim655.7$ mm in Fig. 7 shows the validity of the inference. From Fig. 7 it may be concluded that Eq. (23) describes reasonably well the experimental results.

3. 4. Turbulent properties

Particular slanted probe designed to minimize the effect of the prong wake on the wire has been used and attention has been payed to keep the same condition for the two runs once for the I-probe and the next for the slanted probe. However the scatter of the data obtained by this method was rather large and many experiments have been performed to gather reliable data.

Figures 8 (a), (b), (c) show the variations of turbulent intensity components with the speed ratio at the downstream section $x=655.7$ mm. Reynolds number for $\Omega_m=0$ is 8×10^4 and it is constrained to 4×10^4 at $\Omega_m=2$ and 3 because of the upper limit of the rotating speed of the apparatus. Each turbulent intensity component is represented by two types of non-dimensional forms. The one uses the main flow velocity and this shows the absolute change in turbulent intensities. The other uses the relative velocity $U_{R0}=\sqrt{U_e^2+V_0^2}$. This non-dimensional form is introduced

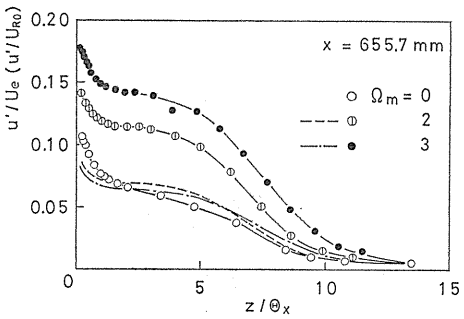

Fig. 8. (a) Variation of u-component of turbulent intensity with the speed ratio.

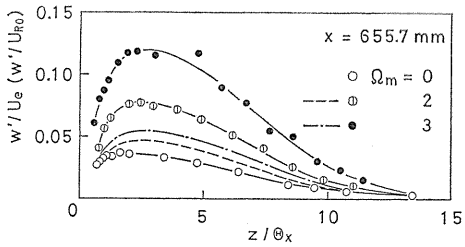

Fig. 8. (b) Variation of v-component of turbulent intensity with the speed ratio.

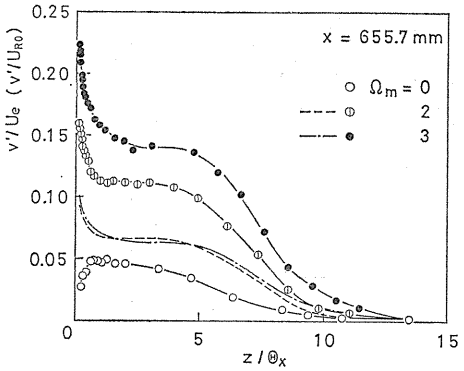

Fig. 8. (c) Variation of w-component of turbulent intensity with the speed ratio.

considering the approximate generalized quasi-collaterality of the mean velocity. Exactly we should take the relative velocity $\sqrt{U_e^2+(r\omega)^2}$ at the point considered as the reference but U_{R0} is used for the sake of convenience.

Figure 8(a) presents u-turbulent intensity distribution. The distribution for the case of $\Omega_m=0$ is practically similar to that of the flat-plate turbulent boundary layer. The rotation of the cone enlarges the intensity expressed by u'/U_e as seen in the figure. But u-turbulent intensities expressed by u'/U_{R0} in the cases of $\Omega_m=2$ and 3 are nearly the same values as in the case of $\Omega_m=0$ and near the wall they even decrease with increase in the speed ratio.

v-turbulent intensity distribution, v'/U_e, shown in Fig. 8(b) also exhibits remarkable increase with the speed ratio. The trend of v'/U_{R0} in the cases of $\Omega_m=2$ and 3 is rather larger than that of $\Omega_m=0$. Especially near the wall v'/U_{R0} in the case of $\Omega_m=0$ decreases, on the other hand v'/U_{R0} in the cases of $\Omega_m=2$ and 3 show rapid increase. Figure 8(c) presents the distribution of turbulent intensity component normal to the wall. w'/U_e shows marked increase with the speed ratio as do the other components. w'/U_{R0} exhibits still larger value with rotation as seen in the figure.

In what follows we will consider the character of the each turbulent intensity distribution by use of the equations for the turbulent energy components following to the previous discussion.[5] These equations are

$$\left.\begin{aligned} D\left(\frac{\overline{u}^2}{2}\right)&=-2\lambda\overline{uv}\frac{V}{R}-\overline{uw}\frac{\partial U}{\partial z}+D_{11}+P_{11}-\varepsilon_u,\\ D\left(\frac{\overline{v}^2}{2}\right)&=2\lambda\overline{uv}\frac{V}{R}-2\overline{vw}\frac{V}{R}-\overline{vw}R\frac{\partial}{\partial z}\left(\frac{V}{R}\right)+D_{22}+P_{22}-\varepsilon_v,\\ D\left(\frac{\overline{w}^2}{2}\right)&=2\overline{vw}\frac{V}{R}+D_{33}+P_{33}-\varepsilon_w, \end{aligned}\right\} \quad (31a,\ b,\ c)$$

where D_{ij} and P_{ij} stand for turbulent diffusion terms and pressure-rate of strain terms respectively and ε_u, ε_v and ε_w represent dissipations of each component. Detail expressions of these terms are presented in the literature.[5] Equation (31a) includes the conventional production term $-\overline{uw}\partial U/\partial z$ and a distinguishing term $-2\lambda\overline{uv}V/R=\lambda T_1$ which interacts with $\overline{v}^2$-component. In the flat-plate turbulent boundary layer we may roughly say that $\overline{v}^2$ is generated only through the pressure-rate of strain redistribution term. On the other hand Eq. (31b) has two interaction terms; one is $-\lambda T_1$ and the other $-2\overline{vw}V/R=-T_2$ indicating the interaction between $\overline{v}^2$ and $\overline{w}^2$. Moreover this equation has a direct production term $-\overline{vw}R\,\partial(V/R)/\partial z$. Equation (31c) of $\overline{w}^2$-component has no production term but a novel interaction term T_2.

On the basis of these equations we can say about the distributions shown in Figs. 8(a), (b) and (c) that the novel term contributes only small amount to u'/U_{R0} but for v'/U_{R0} new production term works and it shows large increase with rotation and the transport term T_2 acts appreciably for w'/U_{R0}. Naturally the rotation of the cone affects the other non-linear terms, D_{ij}, P_{ij} and ε_u, $_v$, $_w$, then the exact role of the each term could be clarified only after the every terms would be measured.

Reynolds shear stress components are shown in Figs. 9 (a), (b) and (c) with Ω_m as a parameter. Figure 9 (a) presents $-\overline{uw}/U_e^2$ relating to τ_{ox}. It increases with

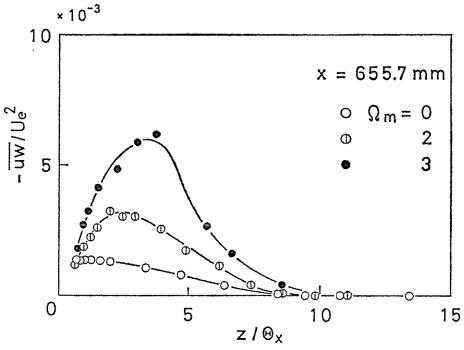

Fig. 9. (a) Reynolds shear stress $-\overline{uw}/U_e^2$.

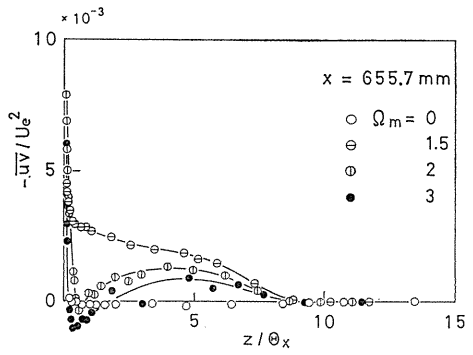

Fig. 9. (b) Reynolds shear stress $-\overline{uv}/U_e^2$.

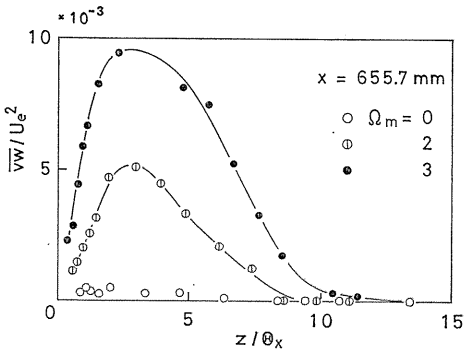

Fig. 9. (c) Reynolds shear stress $\overline{vw}/U_e^2$.

the speed ratio in the middle of the boundary layer and the profiles in the cases of $\Omega_m=2$ and 3 are very different from that of $\Omega_m=0$ but the near-wall region $-\overline{uw}/U_e^2$ of each case coincides irrespective of the value of Ω_m. We have shown the development of this term in the downstream direction and it has shown no large change,[5] but Fig. 9 (a) exhibits very large effect of the speed ratio on this component.

A shear stress $-\overline{uv}/U_e^2$ is shown in Fig. 9 (b). It should be zero in the case of $\Omega_m=0$ due to the symmetry, and the measurement exhibits the existence of this nature in the present flow. When the body rotates at $\Omega_m=1.5$ ($R_e=8\times10^4$), $-\overline{uv}/U_e^2$ is appreciable in the whole layer and it decreases monotonically from the wall region toward the outer layer. The distribution of this component shows drastic change in the case of $\Omega_m=2$. It has very large peak in the proximity of the wall and decreases very rapidly and then shows a mild maximum. This trend is more pronounced in the case of $\Omega_m=3$ and there is a region where $-\overline{uv}/U_e^2$ becomes even negative.

If we explain this distribution by use of a scalar eddy viscosity, we should have zero or negative value of $\partial(V/R)/\partial x$ at some z in the following expression,

$$-\overline{uv}=\nu_T R\frac{\partial}{\partial x}\left(\frac{V}{R}\right). \tag{32}$$

Although there is some possibility of such a situation, we can hardly imagine $\partial(V/R)/\partial x$ takes zero or negative value, because it is at the wall that it takes zero and

because the value of V/R near the wall will usually increase toward downstream in accordance with the growth of the boundary layer. Furthermore, as seen from Fig. 5 which shows the development of the mean velocity distribution, $R\partial(V/R)/\partial x$ does not have such a large value as to be required to explain the peak of $-\overline{uv}/U_e^2$ near the wall.

Figure 9(c) shows the variation of $\overline{vw}/U_e^2$ with Ω_m. The experimental value satisfies the required symmetry condition of $\Omega_m=0$. This shear stress increases remarkably with the speed ratio. $\overline{vw}/U_e^2$ is related τ_{oy} but if the curve of $\overline{vw}/U_e^2$ is extended to the wall, corresponding value of τ_{oy} is too small. This is due to the thickning of the viscous sublayer or the problem of the accuracy of measurement near the wall.

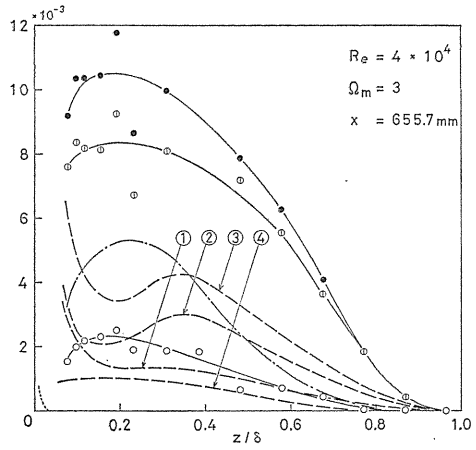

Fig. 10. Turbulent energy production terms and transport terms.
---, $\Omega_m=1.5$. ○, ①, $-(\delta/U_e^3)\overline{uw}\partial U/\partial z$; ①, ②, $-(\delta/U_e^3)\overline{vw}R\partial(V/R)/\partial z$; ●, ③, $-(\delta/U_e^3)\{\overline{uw}\partial U/\partial z+\overline{vw}R\partial(V/R)/\partial z\}$; ——·——, ④, $(\delta/U_e^3)T_2$; ·····, $(\delta/U_e^3)\lambda T_1$.

In Fig. 10 distribution of the turbulent energy production terms which play the most important role in the turbulent energy budget and the characteristic transport terms of this flow are plotted. From the figure it is seen that the novel production term produced by the azimuthal velocity, $-\overline{vw}R\partial(V/R)/\partial z$, is larger than the conventional production term, $-\overline{uw}\partial U/\partial z$. The speed ratio affects the distribution of these terms near the wall, that is, in the case of $\Omega_m=1.5$ these terms are very large near the wall but the distribution for $\Omega_m=3$ does not show such a trend. The transport term T_2 is very important in the whole layer as evident from the figure, but the other transport term λT_1 is limited very near the wall.

Above consideration demonstrates the strong effect of the speed ratio on the turbulence structure of the present flow. Main reason of this process may be the vigour mixing due to the instability of the turbulent fields by the centrifugal force. Macroscopic parameter governing this process is the speed ratio but a local parameter is suitable to describe this phenomenon. Richardson number is an obvious candidate. There are various kinds of Richardson number, however the following flux Richardson number R_f related to the total turbulent energy equation is most useful, that is,

$$D\left(\frac{\bar{q}^2}{2}\right)=\left\{-\overline{uw}\frac{\partial U}{\partial z}-\frac{\overline{vw}}{R}\frac{\partial(RV)}{\partial z}\right\}(1-R_f)+D_f-\varepsilon, \qquad (33)$$

$$R_f=\frac{2\overline{vw}V/R}{\{\overline{uw}\partial U/\partial z+(\overline{vw}/R)\partial(RV)/\partial z)\}}, \tag{34}$$

where D_f and ε are diffusion and dissipation terms respectively.

The variation of the distribution of R_f with the speed ratio is shown in Fig. 11 in the section of $x=655.7$ mm. The absolute value of R_f increases with Ω_m and its maximum in the case of $\Omega_m=3$ reaches twice as large as that of $\Omega_m=2$. This boundary layer increases its instability with increasing the speed ratio.

Finaly a brief discussion will be given of the pressure and the normal stress in the boundary layer. Integration of Eq. (8c) yields

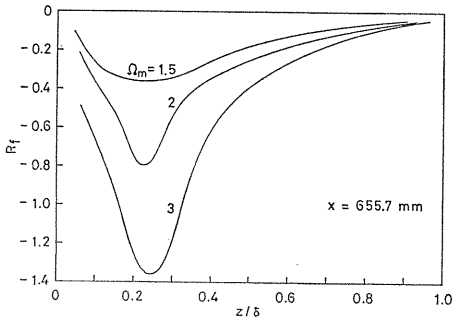

Fig. 11. Change in the flux Richardson number with the speed ratio.

$$\frac{1}{A}\int_z^\delta \frac{A}{R}\left(\frac{V}{V_0}\right)^2 dz=\frac{P_e-P}{\rho V_0^2}+\frac{\overline{w}_e^2-\overline{w}^2}{V_0^2}+\frac{1}{A}\int_z^\delta \frac{A}{R}\frac{\overline{w}^2-\overline{v}^2}{V_0^2}dz. \tag{35}$$

Figure 12 shows various terms of this equation calculated from the experimental values of the highest speed ratio. As discussed in the previous paper[5] the fluctuation terms should be retained in the momentum equation in the z direction.

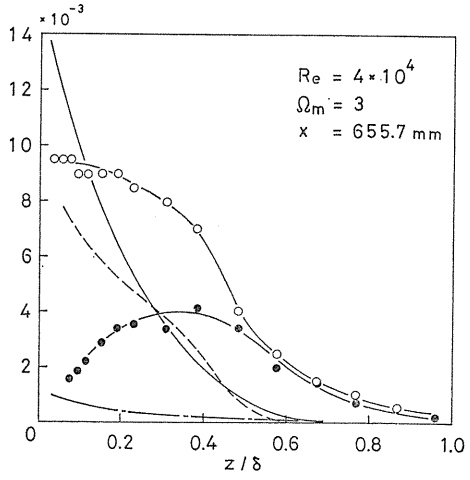

Fig. 12. Various integrated terms of the z-momentum equation.
——, lefthand side of Eq. (35); ---, righthand side of Eq. (35); ○, $(P_e-P)/\rho V_0{}^2$; ●, $-(\overline{w}_e{}^2-\overline{w}^2)/V_0{}^2$; ——·——, $-\frac{1}{A}\int_z^\delta \frac{A}{R}\frac{\overline{w}^2-\overline{v}^2}{V_0{}^2}dz$

4. Concluding Remarks

A study has been carried out on the thick turbulent boundary layer developing on a spinning cone with the radius decreasing in the downstream direction in a constant pressure flow which was realized by a sleeve in the wind tunnel. A very simple calculation method has been devised and also detailed measurements of Reynolds stress have been performed, then the results are summarized as followings.

First, the present simple calculation method predicts momentum thicknesses accurately until $\Omega_m=2$. At $\Omega_m=3$ there is some difference between the theory and the experiment but it seems the error is small enough for the practical purpose. Secondly, the mean velocity distribution makes large change with the speed ratio. This is due to the effect of the inclination of rotating cone surface which acts as an adverse pressure gradient on the boundary layer. This change is clearly seen in the polar plot which deflects downward at the high speed ratio. Thirdly, the turbulent intensity components increase with the speed ratio. If we take the reference velocity as the relative main flow velocity, u-component shows a little difference between the rotating cases and the stationary case but v- and w-components increase with the rotation even expressed by this non-dimensional form. For the process the novel turbulent energy production term and transport terms play important roles. Especially the production term for $\overline{v}^2$ is very large at $\Omega_m=3$. The transport term that transfers the energy from $\overline{v}^2$ to $\overline{w}^2$ is even larger than the usual production term for $\overline{u}^2$. Flux Richardson number also exhibits the vigour effect of the speed ratio. That is, the absolute value of the flux Richadson number increases with the speed ratio showing the instability of the boundary layer. Finally, Reynolds shear stresses $-\rho\overline{uw}$ and $\rho\overline{vw}$ increase with the speed ratio and have a maximum in the middle of the boundary layer. The component $-\rho\overline{uv}$ shows drastic change with the rotation of the cone, and it can not be predicted by a classical eddy viscosity concept.

References

1) Reynolds, W. C., *Annual Review of Fluid Mechanics*, Vol. 8 (1976), 183, Annual Review Inc.
2) Schliching, H., *Boundary Layer Theory*, 7th ed., (1979), 242, McGraw Hill.
3) Parr, O., *Ing.-Arch.*, Bd. 32 (1963), 393.
4) Furuya, Y., Nakamura, I. & Yamashita, S., *Memoirs of the Faculty of Eng.*, Nagoya Univ., Vol. 30, No. 1 (1978), 1.
5) Nakamura, I., Yamashita, S. & Furuya, Y., *Turbulent Shear Flows* 2, ed., Durst, F., et al., (1980), 99, Springer.
6) Arzoumanian, E., Fulachier, L. & Dumas, R., *2nd Symposium on Turbulent Shear Flows*, July, 1979, Imperial College, London, 4. 28.
7) Koosinlin, M. L., Launder, B. E. & Sharma, B. I., *Trans. ASME*, Ser. C, Vol. 96 (1974), 204.
8) Sharma, B. I., *AIAA J.*, Vol. 15 (1977), 271.
9) Launder, B. E., Priddin, C. H. & Sharma, B. I., *Trans. ASME*, Ser. I, Vol. 99 (1977), 231.
10) Higuchi, H. & Rubesin, M. W., *AIAA J.*, Vol. 17 (1979), 931.
11) Hinze, J. O., *Turbulence*, 2nd ed., (1975), 586, McGraw Hill.

12) Kline, S. J., et al., ed., *Computation of Turbulent Boundary Layers*, Vol. 1, (1969), Stanford Univ.
13) Mager, A., *NACA Rep.* 1067 (1952).
14) Furuya, Y. & Nakamura, I., *Trans. ASME*, Ser. E, Vol. 37 (1970), 17.
15) See Ref. 2), p. 676.